photonics

MDPI

Article

Nondestructive Detection of Thermal Aging in XLPE Based on Terahertz Spectroscopy

Junping Cao [1], Wenhui Yan [2], Yiming Zheng [1], Jiayu Liu [2], Zhiyi Gao [3], Baiqiang Sun [2], Yuntu Jiang [4], Yu Ma [1] and Zhenwei Zhang [2,*]

[1] State Grid Zhejiang Electric Power Research Institute, Hangzhou 310014, China; cao_junping1@zj.sgcc.com.cn (J.C.); zheng_yiming@zj.sgcc.com.cn (Y.Z.); ma_yu1@zj.sgcc.com.cn (Y.M.)
[2] Department of Physics, Capital Normal University, Beijing 100048, China; 2240602060@cnu.edu.cn (W.Y.); 2250602065@cnu.edu.cn (J.L.); 2240602071@cnu.edu.cn (B.S.)
[3] State Grid Corporation of China, Beijing 100031, China; zhiyi-gao@zju.edu.cn
[4] State Grid Zhejiang Electric Power Co., Ltd., Hangzhou 310007, China; jiang_yuntu@zj.sgcc.com.cn
* Correspondence: zhangzw@cnu.edu.cn

Abstract

XLPE power cables have become the core insulation material in the power cable industry and are widely used in high-voltage and extra-high-voltage cable systems due to their advantages of large transmission capacity, excellent dielectric properties, and stable physicochemical characteristics. The aging state of XLPE directly affects the safety and stability of power transmission. Therefore, an in-depth analysis of the aging mechanisms, a thorough understanding of the aging patterns, and the establishment of a scientific aging condition assessment framework are of great significance for ensuring the reliable operation of XLPE cables. In this paper, a nondestructive detection study of thermal aging in XLPE is conducted based on terahertz (THz) spectroscopy, focusing on the evolution of optical parameters during the thermal aging process. The research demonstrates that THz spectroscopy can sensitively capture the dynamic changes occurring during the thermal aging of XLPE. This provides a novel technical approach and theoretical support for the nondestructive evaluation of thermal aging in the cable industry. The findings hold substantial theoretical value and practical significance for safeguarding the secure and reliable operation of power cables and preventing electrical accidents.

Keywords: XLPE; thermal aging; terahertz spectroscopy; refractive index; absorption coefficient

1. Introduction

In recent years, China has accelerated the construction of high-voltage, extra-high-voltage, long-distance, and large-capacity power networks. As a vital component of power infrastructure, the technological advancement of power cables directly reflects the level of the nation's electric power industry development. Power cables typically consist of conductors, insulation dielectric, shielding layers, and outer sheaths. Currently, commonly used insulating materials include cross-linked polyethylene (XLPE), polyvinyl chloride (PVC), and ethylene-propylene rubber (EPR). Among these, XLPE has become the preferred insulation material for cables across all voltage levels and is widely employed in high-voltage and extra-high-voltage cable systems due to its excellent electrical characteristics, high breakdown strength, good thermal resistance, and outstanding anti-aging performance [1–3].

Check for updates

Received: 21 April 2026
Revised: 10 May 2026
Accepted: 11 May 2026
Published: 1 July 2026

Copyright: © 2026 by the authors. Licensee MDPI, Basel, Switzerland. This article is an open access article distributed under the terms and conditions of the Creative Commons Attribution (CC BY) license.

However, during long-term operation, XLPE materials gradually age under the combined influence of multiple factors, including electric fields, thermal fields, and mechanical stresses, leading to the deterioration of insulation performance and even breakdown accidents, thereby posing a serious threat to the safe operation of power grids. According to statistical data from the State Grid Corporation of China, among cable failures, those caused by insulation aging account for the highest proportion, exceeding 40% of total faults [4]. Therefore, an in-depth analysis of the aging mechanisms of XLPE cables, a thorough understanding of their aging patterns, and the establishment of a scientific aging condition assessment framework are of great significance for ensuring the reliable operation of XLPE cables.

Currently, nondestructive testing methods for insulating materials primarily include ultrasonic testing [5], infrared thermography [6], X-ray inspection [7], and terahertz (THz) detection, which is still under research investigation. Among these methods, ultrasonic testing is insensitive to internal defects, while infrared thermography is significantly affected by ambient temperature variations. X-ray inspection is a reliable detection method, yet it is prone to overexposure in low-density, lightweight insulating materials, which can obscure defects, and X-rays pose pathological hazards to human health. In contrast, terahertz detection technology offers distinct advantages, including no requirement for coupling agents, strong penetration capability for non-polar substances, and low photon energy that is harmless to both the human body and materials [8–11].

Terahertz (THz) spectroscopy, as an emerging nondestructive testing technique, possesses unique advantages including non-contact measurement, strong penetration capability, high sensitivity, and the ability to acquire abundant physical and chemical information about materials [12–16]. The frequency range of THz waves coincides with the rotational and vibrational energy level transition frequencies of molecules [17–19], enabling specific interactions with the molecules of XLPE materials and allowing precise detection of changes in molecular structure and intermolecular interactions induced by thermal aging, oxidation, and other factors [19]. In 2019, Mei et al. [20] employed a terahertz time-domain spectroscopy (THz-TDS) system and a broadband dielectric spectrometer to test five commonly used insulating materials: epoxy resin, epoxy glass fiber, XLPE, electrical porcelain, and high-temperature vulcanized (HTV) silicone rubber. In 2020, In-Sung Lee et al. [21] utilized a continuous-wave (CW) terahertz imaging system to detect internal defects in XLPE sheets used for power cable insulation. Through two-dimensional images of THz waves transmitted through the XLPE sheets, defects with a diameter of approximately 0.5 mm could be identified. In 2022, Nsengiyumva et al. [22] investigated the terahertz spectral characteristics of five different electrical insulating materials (PER, GFRP, XLPE, E-PRL, and HTVSR) and analyzed the relationships between these electromagnetic parameters and factors such as polar groups within the material system, molecular rigidity, ambient temperature, and molecular chain structure and symmetry. The aforementioned studies provide new methodologies and theoretical foundations for the aging assessment and defect detection of XLPE insulating materials.

This paper focuses on the challenge of assessing the thermal aging state of XLPE power cables. By employing THz spectroscopy, a systematic investigation is conducted into the evolution of the optical properties of XLPE subjected to thermal aging treatment at 155 °C for varying durations. As the aging duration increases to 18 days, both the time-domain signals and the frequency-domain spectral amplitudes of XLPE exhibit a marked decrease. Correspondingly, parameters including the refractive index and the extinction coefficient demonstrate significant variations throughout the aging process.

2. Sample Preparation

The cable samples utilize a domestic high-performance cross-linked polyethylene (XLPE) insulation material system, with a rated voltage level of 500 kV and a conductor cross-sectional area of 2500 mm^2, classifying them as extra-high-voltage, large-section power cables. The conductor is designed with a stranded structure of high-conductivity metallic materials, balancing current-carrying capacity and mechanical properties, thereby rendering it suitable for large-capacity, long-distance power transmission scenarios. The cable insulation layer employs XLPE material characterized by high purity and strictly controlled impurity content. Through the optimization of the cross-linking process and structural design, the electrical performance and long-term operational stability are effectively enhanced.

Regarding operational parameters, the cable design permits a continuous long-term operating temperature of 90 °C for the conductor and can withstand certain short-term overload conditions. The insulation material is designed and validated for a long-term thermal aging life of no less than 40 years, with comprehensive consideration given to the effects of coupled thermal, electrical, and mechanical fields on material performance. This ensures the maintenance of stable dielectric and mechanical properties throughout the long-term service life.

In terms of the material system, a composite antioxidant stabilization system is incorporated into the insulation compound, involving the synergistic configuration of primary and secondary antioxidants. This effectively inhibits thermo-oxidative degradation during processing and operation, enhancing the material's thermal stability and aging resistance. Furthermore, by controlling cross-linking by-products, regulating the microstructure, and optimizing interfacial matching, the accumulation of space charge and the level of dielectric loss are reduced, thereby further improving the overall electrical reliability of the cable.

Additionally, the cable structural design takes full account of the electric field distribution characteristics at the extra-high-voltage level. By optimizing the conductor shield, insulation shield, and geometric structure, uniform electric field control is achieved, reducing the risk of local electric field distortion. The synergistic design of the overall material and structural system endows the cable with excellent long-term operational reliability and suitability for engineering applications.

The experimental samples were obtained from a domestic 110 kV unused commercial XLPE cable, and sheet-like XLPE specimens with a thickness of approximately 1 mm were prepared by slicing. The XLPE sheet specimens were placed in a constant-temperature oven for thermal treatment at an aging temperature of 155 °C. Test samples were prepared sequentially with thermal aging durations increasing day by day from 1 day up to 20 days. Including the unaged original sample, a total of 21 groups of specimens were obtained, and their physical photographs are shown in Figure 1.

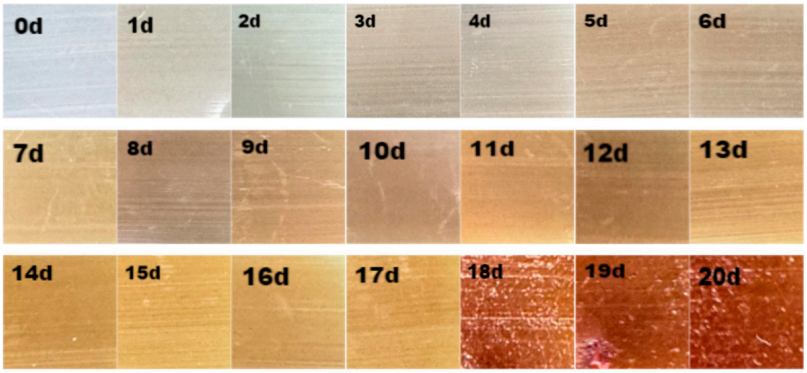


Figure 1. Physical photographs of the samples.

After each sampling, the specimens were promptly placed in a dry, light-proof environment to cool to room temperature, thereby preventing secondary effects of external environmental factors on the material properties. The cooled specimens were properly sealed to guard against moisture ingress or contamination. Table 1 presents the thickness measurement results of the aged samples.

Table 1. Thickness measurements of the aged samples.

Aging Time (d)	Measurement 1 (mm)	Measurement 2 (mm)	Measurement 3 (mm)	Mean Thickness (mm)
0	1.129	1.130	1.126	1.128
1	1.176	1.175	1.170	1.174
2	1.081	1.083	1.082	1.082
3	1.161	1.159	1.156	1.159
4	1.082	1.082	1.082	1.082
5	1.226	1.218	1.224	1.223
6	1.105	1.107	1.107	1.106
7	1.087	1.087	1.087	1.087
8	1.188	1.194	1.189	1.190
9	1.101	1.094	1.094	1.096
10	1.114	1.116	1.114	1.115
11	1.164	1.165	1.163	1.164
12	1.080	1.081	1.080	1.080
13	1.093	1.093	1.091	1.092
14	1.164	1.161	1.161	1.162
15	1.174	1.179	1.176	1.176
16	1.158	1.155	1.160	1.158
17	1.189	1.184	1.186	1.186
18	1.050	1.048	1.051	1.050
19	1.048	1.050	1.046	1.048
20	1.052	1.052	1.047	1.050

3. Experimental System and Principle

Spectral measurements of the thermally aged XLPE samples were performed using a transmission-mode terahertz time-domain spectroscopy (THz-TDS) system. During the experiments, the relative humidity was controlled to $\leq$9% and the room temperature was maintained at 22 °C to suppress the interference of moisture absorption on the terahertz signal. Based on the optical constant extraction models proposed by Dorney [23] and Duvillaret [14], parameters including the complex refractive index and absorption coefficient of the samples were extracted.

The transmission-mode optical parameter extraction method is the most commonly employed approach for analyzing the optical properties of materials in the terahertz frequency range and is primarily suitable for measuring samples with relatively weak terahertz absorption. When conducting measurements with a THz-TDS system, the following assumptions are made: (i) the terahertz wave propagates orthogonally through a planar sample with a homogeneous structure, such that scattering losses and errors due to incident angle can be neglected and (ii) the polarization of the terahertz wave is linear and parallel to the incident optical axis. The macroscopic properties of the material are generally characterized by the complex refractive index $\widetilde{n} = n - i\kappa$, where n is the refractive index, reflecting the dispersion characteristics of the terahertz wave within the material, and κ is the extinction coefficient, representing the absorption characteristics of the material. The

relationship between the extinction coefficient κ and the absorption coefficient α can be expressed as:

$$\alpha = \frac{2\omega\kappa}{c} \tag{1}$$

Here, the parameters n, κ, and α, which are determined by the absorption and dispersion relationships, are all frequency-dependent response functions; ω denotes the angular frequency of the THz wave; and c represents the propagation velocity of the terahertz wave in vacuum.

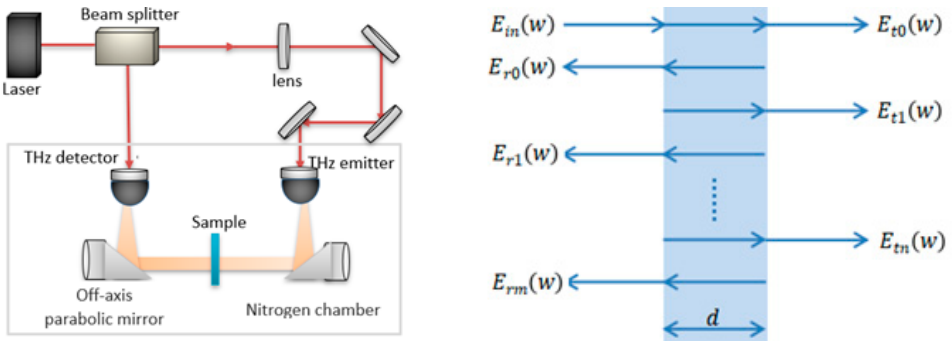
Based on Maxwell's equations and boundary conditions, when an electromagnetic wave interacts with matter, phenomena such as reflection and transmission occur at discontinuous interfaces. As illustrated in Figure 2, a terahertz beam propagates through a sample of thickness d (Medium 2) from Medium 1 to Medium 3. Both Medium 1 and Medium 3 are air, with a refractive index of $n_a = 1.00027 - j0$; the refractive index of the sample is denoted by n_s. The terms t_{as} and r_{as} represent the transmission and reflection coefficients, respectively, of the terahertz wave from air to the front surface of the sample, while t_{sa} and r_{sa} represent the transmission and reflection coefficients, respectively, between the rear surface of the sample and air. These coefficients are all frequency-dependent functions. According to Fresnel's law, the following relationships hold:

$$t_{as} = \frac{2\tilde{n_a}}{\tilde{n_a} + \tilde{n_s}} \tag{2}$$

$$r_{as} = \frac{\tilde{n_s} - \tilde{n_a}}{\tilde{n_a} + \tilde{n_s}} \tag{3}$$

$$t_{sa} = \frac{2\tilde{n_s}}{\tilde{n_s} + \tilde{n_a}} \tag{4}$$

$$r_{sa} = \frac{\tilde{n_a} - \tilde{n_s}}{\tilde{n_s} + \tilde{n_a}} \tag{5}$$



(**a**) (**b**)

Figure 2. (**a**) Transmission-mode working principle schematic; (**b**) Schematic of THz wave transmission through the sample.

Using the THz-TDS system, time-domain information such as the amplitude and phase of the sample is obtained, and the frequency-domain characteristics of the sample are derived via Fourier transformation. In the diagram, the terahertz signals at each interface are represented in the frequency-domain form. $E_{\mathrm{in}}(\omega)$ denotes the incident terahertz signal, $E_{\mathrm{rm}}(\omega)$ represents the terahertz signal after m internal reflections, and $E_{\mathrm{tn}}(\omega)$ denotes the terahertz signal after n transmissions.

Assuming that the propagation distance of the terahertz wave is L when no sample is placed in the optical path, the propagation factor of the terahertz wave in air is expressed as:

$$P_a(L) = exp\left(-j\frac{\widetilde{n_a}\omega L}{c}\right) \tag{6}$$

Similarly, the propagation factor of the terahertz wave within the sample of thickness d is given by:

$$P_s(d) = \exp\left(-j\frac{\widetilde{n_s}\omega d}{c}\right) \tag{7}$$

The terahertz signal measured without a sample in place is defined as the reference signal, denoted by $E_{\mathrm{ref}}(\omega)$, which gives:

$$E_{\mathrm{ref}}(\omega) = E_{\mathrm{in}}(\omega)P_a(L) \tag{8}$$

The terahertz signal acquired after placing the sample in the optical path is defined as the sample signal, denoted by $E_{\mathrm{sam}}(\omega)$. Based on the preceding formulas, the expression for the terahertz signal transmitted through the sample is given by:

$$E_{t0}(\omega) = E_{in}(\omega)\, t_{as}\, t_{sa}\, P_a(L-d)\, P_s(d) \tag{9}$$

$$E_{\mathrm{t1}}(\omega) = E_{\mathrm{in}}(\omega)\, t_{\mathrm{as}}\, r_{\mathrm{as}}^2\, t_{\mathrm{sa}}\, P_a(L-d)\, P_s^3(d) \tag{10}$$

$$E_{t2}(\omega) = E_{in}(\omega)\, t_{as}\, r_{as}^4\, t_{sa}\, P_a(L-d)\, P_s^5(d) \tag{11}$$

$$E_{tn}(\omega) = E_{in}(\omega)\, t_{12}\, r_{as}^{2n}\, t_{23}\, P_a(L-d)\, P_s^{2n+1}(d) \tag{12}$$

The repeated transmission of terahertz waves within the sample is referred to as the Fabry–Perot (FP) effect. The transmitted signal of the sample is the sum of all transmitted echoes and is denoted by $E_{\mathrm{total}}(\omega)$. Therefore, it can be expressed as:

$$E_{\mathrm{total}}(\omega) = E_{\mathrm{in}}(\omega)\, t_{\mathrm{as}}\, t_{\mathrm{sa}}\, P_a(L-d)\, P_s(d) \times \left\{\sum_{i=0}^{n} r_{\mathrm{as}}^2\left[P_s^2(d)\right]^i\right\} \tag{13}$$

From Equations (1)–(13), it can be seen that the expressions for the multiple FP(ω) components described by the FP effect are:

$$FP(\omega) = \sum_{i=0}^{n}\left[r_{\mathrm{as}}^2 P_s^2(d)\right]^i = \frac{1-\left[r_{\mathrm{as}}^2 P_s^2(d)\right]^{n+1}}{1-r_{\mathrm{as}}^2 P_s^2(d)} \tag{14}$$

The complex transfer function of the sample in the terahertz frequency range is defined as the ratio of the sample signal to the reference signal and is denoted by $H(\omega)$. Substituting all parameters into the expression and simplifying yields:

$$H(\omega) = \frac{E_{\mathrm{total}}(\omega)}{E_{\mathrm{ref}}(\omega)} = \frac{4\widetilde{n_s}}{\left(1+\widetilde{n_s}\right)^2}\cdot\exp\left[-j\left(\widetilde{n_s}-1\right)\frac{\omega d}{c}\right]\cdot \mathrm{FP}(\omega) \tag{15}$$

where

$$FP(\omega) = \frac{1-\left[\frac{1-\widetilde{n_s}}{1+\widetilde{n_s}}\right]^{2n+2}\cdot\exp\left[\frac{-j(2n+2)\omega\widetilde{n_s}d}{c}\right]}{1-\left[\frac{1-\widetilde{n_s}}{1+\widetilde{n_s}}\right]^{2}\cdot\exp\left[\frac{-2j\omega\widetilde{n_s}d}{c}\right]} \tag{16}$$

For relatively thin samples, when conducting experiments using a transmission-mode THz-TDS system, the Fabry–Perot (FP) effect within the sample may lead to the overlapping of multiple reflected echoes. This phenomenon complicates the parameter extraction calculations and reduces the accuracy of the results, representing a common issue in time-domain spectral analysis. Consequently, samples of a certain thickness are typically selected for measurement to ensure a clear temporal separation between the main terahertz pulse and its echo interference. By controlling the size of the sampling window during the experiment, it is possible to capture a complete main terahertz pulse signal that is free from echoes. In this case, $i = 0$ and $FP(\omega) = 1$.

Expressing the transfer function $H(\omega)$ in terms of amplitude and phase, with the amplitude denoted by $A(\omega)$ and the phase difference between the reference signal and the sample signal denoted by $\varphi(\omega)$, we have $H(\omega) = A(\omega)\exp[-j\varphi(\omega)]$. The complex refractive index of the sample is given by $\widetilde{n}_s = n_s - i \cdot \kappa_s$. Substituting these expressions into Equation (15) and solving the equation yields:

$$A(\omega) = \frac{4\sqrt{n_s^2 + \kappa_s^2}}{(1 + n_s)^2 + \kappa_s^2} \exp\left(-\kappa_s \frac{\omega d}{c}\right) \tag{17}$$

$$\varphi(\omega) = (n_s - 1) \cdot \frac{\omega d}{c} + \tan^{-1}\left[\frac{\kappa_s}{n_s(1 + n_s) + \kappa_s^2}\right] \tag{18}$$

Assuming the sample is a weakly absorbing material, where the refractive index n_s is much larger than the extinction coefficient κ_s, the approximate solutions for the optical parameters are [24]:

$$n_s = 1 + \phi(\omega) \cdot \frac{c}{\omega d} \tag{19}$$

$$\kappa_s = \ln\left[\frac{4n(\omega)}{\rho(\omega) \cdot [1 + n_s]^2}\right] \cdot \frac{c}{\omega d} \tag{20}$$

$$a_s = -\frac{2}{d} \ln\left[\frac{4n_s(\omega)}{A(\omega)[1 + n_s]^2}\right] \tag{21}$$

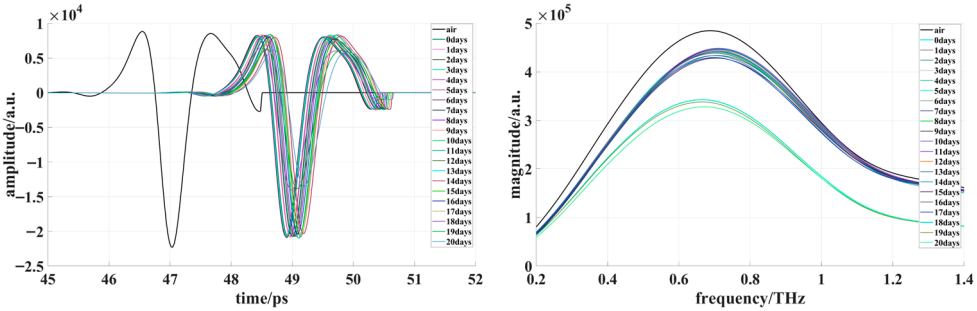
4. Results and Discussion

4.1. Terahertz Spectroscopy Data and Analysis

Figure 3 presents the terahertz time-domain waveform signals of XLPE specimens subjected to different thermal aging durations, along with the corresponding frequency-domain spectral characteristics obtained via fast Fourier transform (FFT). As can be observed from the figure, during the early stage of thermal aging (within 18 days), the signal amplitudes of the XLPE specimens remain relatively high; however, upon entering the later stage of aging (beyond 18 days), the signal amplitudes exhibit a significant attenuation. Concurrently, as the thermal aging duration continues to increase after 18 days, the main peak position of the terahertz time-domain signal for the XLPE specimens shows an overall trend of shifting to the right. Furthermore, within the frequency-domain spectra, the amplitude of the terahertz wave gradually decreases with prolonged aging time. In contrast, prior to 18 days, the amplitude remains relatively stable without evident fluctuations.

Combined with an analysis of the thermal aging mechanism of XLPE materials, short-term thermal treatment typically consumes residual cross-linking by-products within the specimen, thereby reducing the material's absorption of terahertz waves and causing a slight increase in the time-domain signal amplitude [25,26]. However, the XLPE samples employed in this study contain antioxidants, which effectively inhibit the consumption process of cross-linking by-products during the initial aging stage. Consequently, prior to

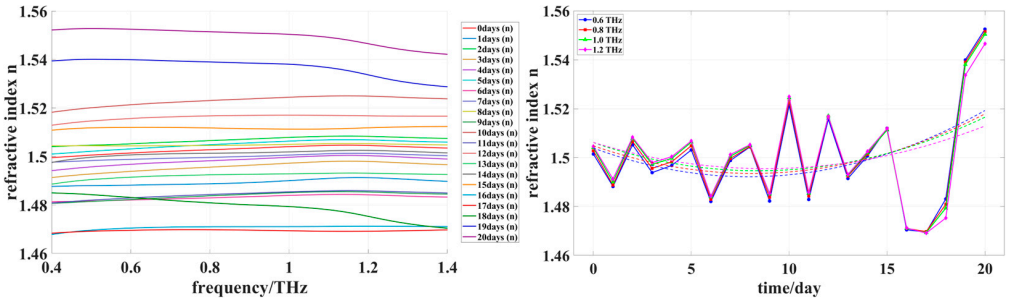
18 days, neither the terahertz time-domain signal intensity nor the absorption coefficient of the material exhibits significant variation. Moreover, the terahertz signal delay times corresponding to samples in different aging states display pronounced differences. This phenomenon directly indicates that the thermal aging process induces microstructural evolution within the XLPE material, ultimately leading to systematic alterations in its refractive index within the terahertz frequency range.



(**a**) (**b**)

Figure 3. (**a**) Terahertz time-domain waveforms and (**b**) frequency spectra of XLPE specimens with different thermal aging times.

Figure 4 presents the terahertz refractive index spectra of XLPE specimens subjected to different thermal aging durations. The results indicate that during the initial stage of thermal aging (within 16 days), the refractive index values of the specimens remain relatively stable across the frequency range without significant fluctuations, suggesting that the macroscopic optical properties of the material are not markedly affected during this phase. When the thermal aging duration falls between 16 and 18 days, the refractive indices of the aged specimens are notably lower than those of the unaged sample within the frequency range of 0.4–1.4 THz. In the later stage of thermal aging (beyond 18 days), as the aging duration further increases, the refractive indices of the XLPE specimens exhibit a gradual upward trend. Based on the overall fitting results, the evolution of the refractive index in the terahertz band with aging time is characterized by a distinct two-stage behavior: an initial decrease followed by a subsequent increase.

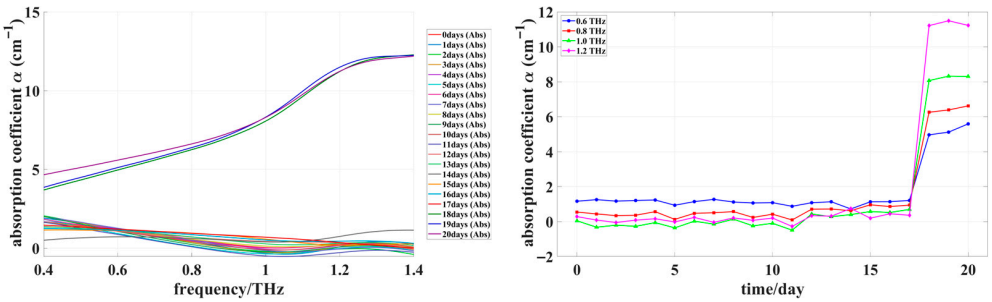


(**a**) (**b**)

Figure 4. (**a**) Refractive index of XLPE specimens subjected to different thermal aging durations; (**b**) Evolution of refractive index with aging time.

Figure 5 displays the terahertz absorption coefficient spectra of XLPE specimens under different thermal aging times. The experimental results show that prior to 18 days of thermal aging, the terahertz absorption coefficients of the XLPE specimens remain stable within the tested frequency range, exhibiting no discernible increasing or decreasing trend. This indicates that thermal aging during this stage does not exert a significant influence on the terahertz absorption characteristics of the material. After the thermal aging duration

exceeds 18 days, the terahertz absorption coefficients of the specimens show a pronounced increasing tendency, and across the entire measured frequency interval, the absorption coefficient gradually rises with increasing terahertz frequency.



(**a**) (**b**)

Figure 5. (**a**) Absorption coefficient of XLPE specimens subjected to different thermal aging durations; (**b**) Evolution of absorption coefficient with aging time.

This indicates that during the initial stage of aging, thermo-oxidative aging affects only the surface of the specimen without inducing changes in its internal structure. After the aging experiment proceeds beyond 18 days, the refractive index increases markedly, suggesting that the hindrance to light propagation by the medium gradually extends from the surface into the interior as the thermo-oxidative reaction progresses. On one hand, the displacement of the electron distribution relative to the nuclear charge centers causes the incident light to be refracted. On the other hand, the disruption of the crystalline structure and the increasing disparity in the distribution of crystalline and amorphous regions further enhance the refraction experienced by light during propagation.

4.2. X-Ray Data and Analysis

Figure 6a presents the X-ray diffraction (XRD) patterns of samples subjected to different aging durations. The diffuse peak near a diffraction angle of 22°, designated as Peak 1, corresponds to the non-crystalline diffraction peak associated with the amorphous region within the XLPE. The two sharper diffraction peaks located near 23° and 25°, designated as Peak 2 and Peak 3, respectively, are crystalline diffraction peaks corresponding to the (110) and (200) crystal planes of the orthorhombic phase in XLPE. As the aging duration increases, both the intensity and the integrated area of the sharp peaks (Peak 2 and Peak 3) exhibit a marked increase, a trend that becomes more pronounced with prolonged aging. This observation indicates that the degradation of the crystalline structure progressively intensifies during the later stages of aging.

As the aging days increase, the insulation performance of XLPE gradually deteriorates. Experimentally, it is observed that the refractive index and absorption coefficient of the material exhibit an obvious mutation at 18 days. Reference [27] shows that the antioxidant content decreases continuously with aging time and, when it drops to a critical value, causes a sudden change in material properties. We think we speculate that the observed 18-day threshold is closely related to the depletion of the antioxidant. Furthermore, reference [28] employs FTIR and XRD to evaluate chemical structural and morphological changes, revealing that thermo-oxidative degradation significantly increases the carbonyl index. Combined with our own XRD microstructural characterization results, both microscopic and macroscopic indicators confirm that high-temperature aging significantly affects the performance behavior of XLPE, and thermo-oxidative degradation may be one of the important chemical mechanisms leading to performance deterioration.

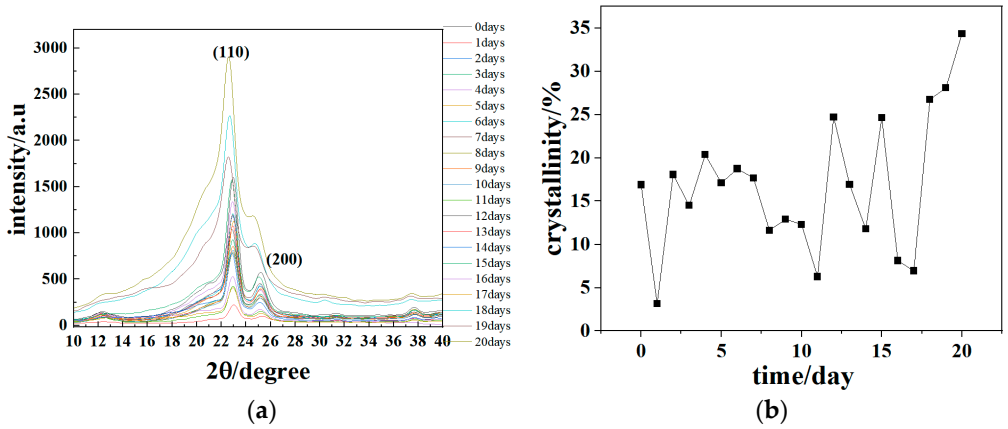


Figure 6. XRD patterns (**a**) and crystallinity (**b**) of XLPE specimens subjected to different thermal aging durations.

5. Conclusions

This paper uses terahertz spectroscopy to detect XLPE samples with different thermal aging durations and systematically analyzes the variation patterns of refractive index and absorption coefficient with XLPE thermal aging time.

This paper conducts nondestructive testing research on XLPE specimens subjected to thermal aging at 155 °C for different durations based on terahertz spectroscopy, and systematically analyzes the evolution of terahertz time-domain and frequency-domain signals, as well as optical parameters such as refractive index and absorption coefficient, during the thermal aging process. The results show that 18 days of thermal aging is a critical point at which the optical properties of XLPE materials undergo significant changes: before 18 days, the terahertz time-domain signal amplitude, frequency-domain amplitude, and absorption coefficient of the specimens remain stable without notable fluctuations; after 18 days, the time-domain signal amplitude attenuates significantly and the main peak position shifts to the right, the frequency-domain amplitude continues to decrease with prolonged aging, the refractive index exhibits a phased increasing trend, and the absorption coefficient rises markedly and increases with higher terahertz frequency. Terahertz spectroscopy can sensitively capture the dynamic changes in optical parameters caused by microstructural evolution during XLPE thermal aging, enabling effective identification of the thermal aging state of XLPE.

This study validates the feasibility and effectiveness of terahertz spectroscopy in the nondestructive detection of thermal aging in XLPE cables, providing a new technical approach and experimental basis for non-contact evaluation of XLPE cable insulation conditions in the power industry. Future work can further investigate terahertz detection of XLPE thermal aging under different temperature conditions, establish quantitative correlation models between optical parameters and XLPE insulation performance, and provide more practical theoretical support and technical methods for condition-based maintenance and life prediction of power grid cable equipment.

Author Contributions: Conceptualization, J.C. and Z.Z.; methodology, J.C., W.Y., Y.Z., Z.G., B.S., Y.J., Y.M. and Z.Z.; software, J.C., W.Y., J.L., B.S., Y.J. and Z.Z.; validation, Z.Z.; investigation, J.C., W.Y., Y.Z., J.L., Z.G. and Z.Z.; resources, J.L.; data curation, Y.Z. and Y.M.; writing—original draft preparation, J.C. and W.Y.; writing—review and editing, Z.Z.; visualization, Z.G. and B.S.; supervision, Z.Z.; project administration, Z.Z.; funding acquisition, Z.Z. All authors have read and agreed to the published version of the manuscript.

Funding: This work was supported by State Grid Zhejiang Electric Power Co., Ltd. Science and Technology Project (B311DS26A009).

Data Availability Statement: The data presented in this study are available on request from the corresponding author due to the authors' desire to better understand the research background and interests of those seeking the data.

Conflicts of Interest: Authors J.C., Y.Z. and Y.M. were employed by the company State Grid Zhejiang Electric Power Research Institute. Author Z.G. was employed by the company State Grid Corporation of China. Author Y.J. was employed by the company State Grid Zhejiang Electric Power Co., Ltd. The remaining authors declare that the research was conducted in the absence of any commercial or financial relationships that could be construed as a potential conflict of interest.

Abbreviations

The following abbreviations are used in this manuscript:

XLPE	Cross-Linked Polyethylene
THz-TDS	Terahertz Time-Domain Spectroscopy
XRD	X-ray Diffraction

References

1. Zhang, S. *High-Performance Cable Materials and Their Application Technologies*; Shanghai Jiao Tong University Press: Shanghai, China, 2015.
2. Saleh, M.A.; Alquennah, A.N.; Ghrayeb, A.; Refaat, S.S.; Abu-Rub, H.; Khatri, S.P. A Review on the Lifetime Estimation Methods of XLPE Power Cables. *IEEE Open J. Ind. Appl.* **2025**, *6*, 445–489. [CrossRef]
3. Emdadi, K.; Gandomkar, M.; Aranizadeh, A.; Vahidi, B.; Mirmozaffari, M. Overview of Monitoring, Diagnostics, Aging Analysis, and Maintenance Strategies in High-Voltage AC/DC XLPE Cable Systems. *Sensors* **2025**, *25*, 7096. [CrossRef] [PubMed]
4. Xue, C. Research on Assessment Method for Insulation Aging State of XLPE Cables. Master's Thesis, Tianjin University, Tianjin, China, 2014.
5. Jodhani, J.; Handa, A.; Gautam, A.; Ashwni; Rana, R. Ultrasonic non-destructive evaluation of composites: A review. *Mater. Today Proc.* **2023**, *78*, 627–632. [CrossRef]
6. Zhu, J.; Mao, Z.; Wu, D.; Zhou, J.; Jiao, D.; Shi, W.; Zhu, W.; Liu, Z. Progress and Trends in Non-destructive Testing for Thermal Barrier Coatings Based on Infrared Thermography: A Review. *J. Nondestruct. Eval.* **2022**, *41*, 49. [CrossRef]
7. Rahman, M.S.U.; Hassan, O.S.; Mustapha, A.A.; Abou-Khousa, M.A.; Cantwell, W.J. Inspection of thick composites: A comparative study between microwaves, X-ray computed tomography and ultrasonic testing. *Nondestruct. Test. Eval.* **2024**, *39*, 2054–2071. [CrossRef]
8. Fattinger, C.; Grischkowsky, D. Terahertz beams. *Appl. Phys. Lett.* **1989**, *54*, 490–492. [CrossRef]
9. Wang, Q.; Xie, L.; Ying, Y. Overview of imaging methods based on terahertz time-domain spectroscopy. *Appl. Spectrosc. Rev.* **2022**, *57*, 249–264. [CrossRef]
10. Wang, Y.; Li, H.; Ge, M.; Xu, D. Terahertz Imaging Technology and Its Application. *Laser Optoelectron. Prog.* **2023**, *60*, 1811004.
11. Wietzke, S.; Jansen, C.; Reuter, M.; Jung, T.; Kraft, D.; Chatterjee, S.; Fischer, B.; Koch, M. Terahertz spectroscopy on polymers: A review of morphological studies. *J. Mol. Struct.* **2011**, *1006*, 41–51. [CrossRef]
12. Krumbholz, N.; Hochrein, T.; Vieweg, N.; Hasek, T.; Kretschmer, K.; Bastian, M.; Mikulics, M.; Koch, M. Monitoring polymeric compounding processes inline with THz time-domain spectroscopy. *Polym. Test.* **2009**, *28*, 30–35. [CrossRef]
13. Sommer, S.; Probst, T.; Kraus, E.; Baudrit, B.; Town, G.E.; Koch, M. Cure monitoring of two-component epoxy adhesives by terahertz time-domain spectroscopy. *Polym. Sci. Ser. B* **2016**, *58*, 769–776. [CrossRef]
14. Duvillaret, L.; Garet, F.; Coutaz, J.L. Highly precise determination of optical constants and sample thickness in terahertz time-domain spectroscopy. *Appl. Opt.* **1999**, *38*, 409. [CrossRef] [PubMed]
15. Stoik, C.; Bohn, M.; Blackshire, J. Nondestructive evaluation of aircraft composites using reflective terahertz time domain spectroscopy. *NDTE Int.* **2010**, *43*, 106–115. [CrossRef]
16. Banks, H.T.; Gibson, N.L. Void detection in foam with knitlines using THz pulse interrogation. *Math. Comput. Model.* **2006**, *44*, 807–815. [CrossRef]
17. Cao, A.D.; Yu, Y.; Song, C.B.; Zhao, Y.M. The present status and tendency of Terahertz spectral detection technology. *J. Telem. Track. Command.* **2020**, *41*, 1–10.
18. Ozaki, T.; Blanchard, F.; Sharma, G.; Razzari, L.; Ropagnol, X.; Vidal, F.; Morandotti, R.; Kieffer, J.-C.; Reid, M.; Hegmann, F. THz imaging and spectroscopy using intense THz sources at the advanced laser light source. *Phys. Procedia* **2010**, *5*, 119–124. [CrossRef]
19. Ferguson, B.; Zhang, X.C. Materials for terahertz science and technology. *Physics* **2003**, *32*, 286–293.

20. Mei, H.; Li, L.; Yin, F.; Hu, W.; Liu, J.; Wang, L. Research on the Dielectric Properties Detection of Typical Electrical Insulation Materials by Terahertz Wave Spectroscopy. *IEEE Access* **2019**, *8*, 226887–226896.
21. Lee, I.S.; Lee, J.W. Nondestructive internal defect detection using a CW–THz imaging system in XLPE for power cable insulation. *Appl. Sci.* **2020**, *10*, 2055. [CrossRef]
22. Nsengiyumva, W.; Zhong, S.; Wang, B.; Zheng, L.; Zhang, Z.; Zhang, Q.; Zhong, J.; Luo, M.; Peng, Z. Terahertz spectroscopic study of optical and dielectric properties of typical electrical insulation materials. *Opt. Mater.* **2022**, *123*, 111837. [CrossRef]
23. Dorney, T.; Baraniuk, R.; Mittleman, D. Material parameter estimation with terahertz time-domain spectroscopy. *J. Opt. Soc. Am. A Opt. Image Sci. Vis.* **2001**, *18*, 1562–1571. [CrossRef] [PubMed]
24. Zhang, Z.; Jia, R.; Xu, J.; Niu, Q.; Yang, Y.; Zhang, C.; Zhao, Y. Quasi-optical measurement and complex refractive index extraction of flat plate materials using single time-domain transmission model in Y-Band. *IEEE Trans. Microw. Theory Tech.* **2022**, *70*, 5224–5233. [CrossRef]
25. Luo, X.; Wang, G.; Nie, M.; Lv, W.; Xie, W. Numerical investigation of terahertz wave propagation in XLPE cable insulation for nondestructive defect detection. In *Proceedings of the AOPC 2025: Infrared and Terahertz Technology and Applications, Beijing, China, 24–27 June 2025*; SPIE: Bellingham, WA, USA, 2025; Volume 13957.
26. Xu, N.; Zhong, L.; Sui, R.; Ahmed, M.; Li, F.; Liu, Y.; Gao, J. Correlation between Terahertz Dielectric Properties of XLPE and Its Composition Structure during Electrothermal Aging. *Macromolecules* **2022**, *55*, 8186–8194. [CrossRef]
27. Zheng, Y.; Long, Y.; Yi, D.; Zhang, H.; Gao, J.; Wu, K.; Li, J. Correlation between antioxidant depletion kinetic model and ageing behaviour of cross-linked polyethylene cable insulation. *High Volt.* **2023**, *8*, 231–238. [CrossRef]
28. Smaida, A.; Mecheri, Y.; Boukezzi, L.; Bouazabia, S. Mechanical behavior of 60 kV HV XLPE insulation under thermal aging and cross-correlation assessment of degradation mechanisms. *J. Mech. Sci. Technol.* **2025**, *39*, 611–625. [CrossRef]

Disclaimer/Publisher's Note: The statements, opinions and data contained in all publications are solely those of the individual author(s) and contributor(s) and not of MDPI and/or the editor(s). MDPI and/or the editor(s) disclaim responsibility for any injury to people or property resulting from any ideas, methods, instructions or products referred to in the content.